



<https://doi.org/10.15407/ufm.23.02.337>

**M.O. VASYLYEV<sup>1,\*</sup>, B.M. MORDYUK<sup>1,2,\*\*</sup>, S.M. VOLOSHKO<sup>2</sup>, and P.O. GURIN<sup>3</sup>**

<sup>1</sup> G.V. Kurdyumov Institute for Metal Physics of the N.A.S. of Ukraine,  
36 Acad. Vernadsky Blvd., UA-03142 Kyiv, Ukraine

<sup>2</sup> National Technical University of Ukraine  
'Igor Sikorsky Kyiv Polytechnic Institute',  
37 Peremohy Ave., UA-03056 Kyiv, Ukraine

<sup>3</sup> P.L. Shupyk National Healthcare University of Ukraine,  
9 Dorogozhytska Str., UA-04112 Kyiv, Ukraine

\* vasil@imp.kiev.ua, \*\* mordyuk@imp.kiev.ua

## **MICROSTRUCTURE OF Co–Cr DENTAL ALLOYS MANUFACTURED BY CASTING AND 3D SELECTIVE LASER MELTING**

The review analyses the microstructure of the commercial Co–Cr–(Mo, W) dental alloys fabricated by 3D digital selective laser melting (SLM), which is the most promising technique among the emerging additive fabrication technologies used for metal products manufacturing in dentistry. In this regard, the main goal is to compare the microstructures of the metal dental products produced by two currently used technologies, namely, conventional casting and SLM. We consider the latest research published from 2013 to 2022. The microstructures are evaluated using optical microscopy (OM), scanning electron microscopy with energy-dispersive x-ray spectroscopy (SEM–EDS), x-ray diffractometry (XRD), electron backscatter diffraction (EBSD) pattern analysis, and atomic force microscopy (AFM). The microstructure analysis allows concluding whether the SLM fabrication process is suitable for dental applications. As shown, the microstructure of the Co–Cr dental alloys depends on both the chemical composition of the samples and the parameters of the manufacturing technique used. Experimental results have proven that, in contrast to the conventional casting, the SLM-fabricated specimens display superior microstructure due to complete local melting and rapid solidification. Additionally, the SLM process minimizes residual flaws and porosity. As a result, SLM allows producing the dense material comprising homogeneous fine-grain microstructure.

**Keywords:** additive manufacturing technologies, 3D laser melting, microstructure, Co–Cr alloys, dentistry.

Citation: M.O. Vasylyev, B.M. Mordyuk, S.M. Voloshko, and P.O. Gurin, Microstructure of Co–Cr Dental Alloys Manufactured by Casting and 3D Selective Laser Melting, *Progress in Physics of Metals*, **23**, No. 2: 337–359 (2022)

## **1. Introduction**

Dental prosthetics (prosthodontics) is one of the most important areas of the dentistry, which is associated with replacing of the missing tooth/teeth using of the artificial dental treatments. These include fixing of the dentures, veneers, bridges, crowns, implants, and more that can be removable or permanently attached in the patient's mouth. The average biting force of the natural human teeth is approximately 77 kg in the posterior part of mouth and approximately 0.193 GPa on the single cusp of the molar tooth [1]. In this regard, the materials of the dentures must possess the sufficiently high strength. Until now, metal alloys are the most demanded for these purposes.

Many different types of alloys are now available in the market to be used in the prosthodontics (Table 1). It should be noted that, compared with metal alloys the pure metals do not have enough combination of the strength, modulus of elasticity, wear resistance and biologic compatibility for a long-term survival in the mouth as prosthesis. The biocompatibility (inert in the oral environment) of the dental alloys is the critical issue because these materials are in intimate contact with oral tissues for long terms. The historical development of the metallic materials in dentistry was influenced by the following most important factors: the technological changes of the dentures, the progress in metallurgy and the changes in the precious metals price. In particular, during the 20th century, the history of the dentistry has intimately been linked with non-precious metal alloys due to the increasing cost of the noble metals and manufacturing of the metal-ceramic dentures and crowns (Table 1).

In recent years, Co–Cr-based alloys are almost exclusively used for the production of the metallic dental prostheses. These are as possible alternatives to Ni–Cr alloys for the restorations production, since they are free from the risk of Ni-related allergic responses and/or Be-related toxic aggravation. Now Co–Cr alloys are among the best-known base metal alloys in dentistry with various and successful clinical applications [2, 3].

The high strength and stainless nature of the ternary Co–Cr–Mo and Co–Cr–W alloys, first patented in 1907 by Haynes, led to the development of the compositional variants of the Co-based alloys for clinical applications such as artificial knee and hip joints [4]. In dentistry, the first use of the Co-based alloy for investment casting is reported to have started in 1936 [5]. Most of the Co–Cr alloys currently used in industrial and biomedical fields evolved from the work of Elwood Haynes at the turn of previous century. Initially, he demonstrated that the binary Co–Cr (30% Cr, 5% Mo with small portions of Ni and C) alloy possesses high strength and resists stain, and he subsequently identified

Mo and tungsten as powerful strengthening agents for these alloys. Because of their stainless nature and permanent ‘star-like’ lustre, Haynes named them *Stellite alloys*, based on the Latin word *Stella*, which means ‘star’ [6]. The first known dental application of Co–Cr alloys (along with Ni–Cr alloys) was in the 1930s, for the fabrication of removable partial denture (RPD) frameworks. Since then, both Co–Cr and Ni–Cr base-metal alloys have become increasingly popular compared with conventional Type IV gold alloys, which were predominant metals previously used for RPD framework fabrication [6, 7]. The use of Co–Cr-based alloys for metal-ceramic applications was first mentioned in the 1959 M. Weinstein patent (U.S. Pat. No. 3,052,982 Fused porcelain-to-metal teeth 1959) for dental porcelain. The elemental composition that was suggested in that patent was (in wt.%): Co 62.55, Cr 27.00, Mo 6.00, Ni 2.00, Fe 1.00, Si 0.60, Mn 0.60, and C 0.25. Table 2 shows the chemical composition of the modern commercial dental alloys. Cobalt is the main constituent in the alloys presented in Table 2. According to the phase diagram the properties of Co–Cr dental alloys depend on the ratio between  $\gamma$ (f.c.c.)/ $\epsilon$ (h.c.p.) phases and the type, quantity and distribution of the carbide phase in the microstructure [9, 10, 11]. The high content of carbon makes the alloy highly wear resistant mainly due to the  $M_{23}C_6$ ,  $M_7C_3$ , and  $M_6C$  carbides (where  $M$  represents Co, Cr, Mo or W) that form throughout their structure during solidification [12].

**Casting.** Traditionally, the lost-wax casting and hot forging processes are usually used to produce Co-based alloy dental prostheses. Such components with the complex shape can be produced through the casting process, but their strength is not high enough. This is a time con-

**Table 1.** Classification of dental alloys [1]

Metal type	All-metal prostheses	Metal ceramic prostheses	Partial denture frameworks
High noble (HN)	Au–Pd–Cu–Ag Au–Pd–Cu–Ag HN metal ceramic alloys	Au–Pt–Pd Au–Pd–Ag (5–12 wt.% Ag) Au–Pd–Ag (> 12 wt.% Ag) Au–Pd	Au–Ag–Cu–Pd
Noble (N)	Ag–Pd–Au–Cu Ag–Pd N metal ceramic alloys	Pd–Au Pd–Au–Ag Pd–Ag Pd–Cu–Ga Pd–Ga–Ag	
Predominantly base metal	Ti–Al–V Ni–Cr–Mo–Be Ni–Cr–Mo Co–Cr–Mo Co–Cr–W Cu–Al	Ti–Al–V Ni–Cr–Mo–Be Ni–Cr–Mo Co–Cr–Mo Co–Cr–W	Ti–Al–V Ni–Cr–Mo–Be Ni–Cr–Mo Co–Cr–Mo Co–Cr–W

suming process with many steps where errors can occur. The strength of the components produced by plastic deformation can be high enough, but complex shapes are difficult to obtain by forging. Therefore, it is difficult to fabricate the Co-based alloy dental components with both the high strength and complex shape by the conventional process. Also, Co–Cr alloys are more difficult to cast than precious alloys due to their higher melting point (1623–1723 K) and more difficult to the post-process due to their hardness, prone to distortions during solidification phase when they are processed with conventional methods [13–15].

**Additive manufacturing.** In order to solve problems with the traditional casting and closed die forging processes, currently additive manufacturing (AM) is being accepted as the novel candidate for the fabrication of the customized dental, which is receiving increasing attention around the world. AM technology (or 3D printing) creates 3D products layer by layer in the single stage directly from their 3D computer-aided design (CAD) usually by successively adding materials in the layer-by-layer fashion [16–20]. This method is in contrast to the traditional subtractive manufacturing (milling, welding, casting, forming, forging and turning) which based on the mechanical removal of the unneeded material part in order to form the desired component with complex geometries. Now, materials available for 3D printing include plastic poly-

Table 2. Composition of some alloys applied in dentistry (mas.%) [8]

Type	Trade mark	Co	Cr	Mo	Si	Mn	C	Fe	W
Alloys for removable partial denture	Wironit® extrahart Bego (Germany)	63.0	30.0	5.0	1.0	1.0	<1.0		
	Remanium® GM 800 + Dentaurnum (Germany)	58.3	32.0	6.5	1.0		<1.0		1.5
Orthodontic wires	Alloy CoCr 3.002 Dentaurnum (Germany)	31.0–35.0	28.0–32.0	4.0–6.0	≤0.1	≤0.1	≤0.35	27.0–31.0	
	Remaloy® Dentaurnum (Germany)	rest	18.0–22.0	3.0–5.0	≤0.5	≤1.0	≤0.03	4.0–6.0	3.0–5.0
Alloys for fixed prostheses	CoCr Biostar ERNST HINRICHS Dental (Germany)	61.65	27.75		1.61	<1.0		<1.0	8.45
	Vi-comp II® Dentsply Sirona (USA)	52.5	27.4		<1.0			1.0	12.1

mers, metals, and biomaterials among many others. After more than 25 years of the research, development and use this production technology is currently at the starting point of triggering the new industrial revolution in the world, in particular in various industrial domains, such as military, aerospace, automobile and medical, continues to grow with the addition of the new technologies, methods and application [21, 22].

The first automatic method for fabricating of the three-dimensional plastic model with photo-hardening polymer was built in 1981 by Hideo Kodama in Nagoya Municipal Industrial Research Institute (Japan). He was the first to describe a layer-by-layer approach to manufacturing. He came up with a layer-by-layer approach for manufacturing, using the photopolymers that was polymerized by UV light to build the 3D object [23]. Since then, AM has become one of the biggest technology disrupters in the 4<sup>th</sup> industrial revolution.

**3D dental metals printing.** During the development stage in the 1990s, 3D printing was mostly used for rapid prototyping and rapid tooling which involved only polymer and thermoplastic materials. However, advancement in laser and electron beam technologies has contributed to fabricate metallic components. The basic idea of the 3D metals printing was laid down in 1971 in patent by P. Ciraud [24] who can be considered the precursor of the 3D laser cladding processes. The concept of the 3D metals printing using selective laser sintering (SLS) and selective laser melting (SLM) systems first described in the 1977 patent by R. Housholder [25]. Now the metals 3D printing is popular in many industries allowing the printing of the complex metal parts with the relatively low price when compared to traditional manufacturing processes, in particular in the aerospace, automotive, marine, military and medical sectors. Metal 3D printing also has been used in the medical sector such as in creating implants, especially in dental prosthetics. Metal 3D printing materials include stainless steel, Co–Cr alloys, Al alloys, Ni alloys, Ti, and others [26–30].

**Dental medical parts.** The large number of the publications has shown that AM 3D procedure provides the efficient and fast technique to digitally design and manufacture biocompatible metal frameworks for complex dental prostheses with improved physical and chemical properties, such as strength, durability and corrosion resistance with not so high metal release. Nowadays additive manufacturing SLM is the most frequently have been used to develop frameworks in dentistry to fabricate directly metallic dental medical parts from the stainless steel,  $Ti_6Al_4V$ , and the Co–Cr alloys system [31–39]. SLM has the potentiality to substitute traditional techniques for the production of the implanted medical devices and the dental prostheses.

**SLM.** Among the additive methods, SLM as the recently introduced technique has attracted the worldwide interest of research groups for

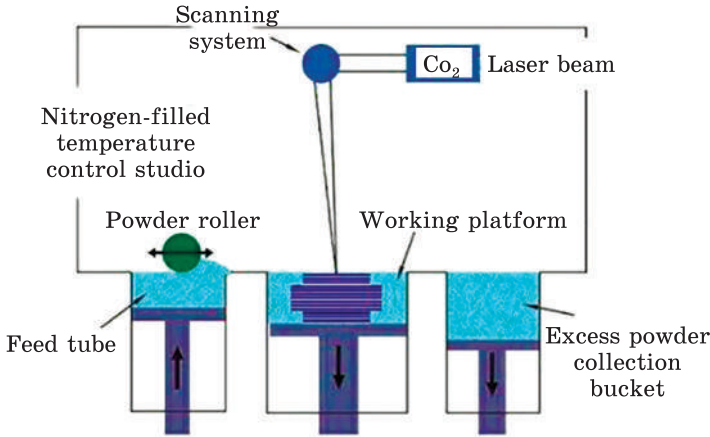


Fig. 1. The SLM process [44]

the manufacturing of the dental metallic structures, such as dental implants, crowns, bridges and prosthetic group with complex geometry [40–43]. In the prosthetic dentistry, the most studies on SLM have focused on Co–Cr dental alloys (see presented review) which have been used to manufacture prosthetic dentistry. Studies have also shown that the SLM-manufactured Co–Cr prostheses have better corrosion resistance and higher strength as compared to those fabricated with conventional casting methods.



Fig. 2. Dental parts fabricated by SLM [45]

SLM is the additive manufacturing procedure that allows printing the metal component directly from the 3D computer-aided design (CAD) by fusing fine metal powder in layers by the high-power laser beam quickly and precisely (Fig. 1). Metal powders used in 3D printing need to be spherical and have a stringent particle size distribution to achieve good packing behaviour. The powders for the next layer are covered on the melted layer, and the laser is again scanned according to the next sliced data. This sequence continues until the near net shape of the products is formed automatically. SLM has the ability to melt fully metal into the solid 3D structure [44]. Figure 2 shows an example of the fabricated dental parts fabricated by SLM.

The main goal of this review is to compare of the microstructures of the metal dental products produced by two currently used technologies, namely conventional casting and SLM. We consider the latest studies published from 2013 to 2022, arranging them in a chronological order.

## 2. Experiment and Discussion: 2013–2022

**2013.** The first comparative analysis of the microstructure Co–29Cr–6Mo alloy specimens fabricated by SLM and conventional casting was performed by the authors of Ref. [46]. The important aspect of this work is the study of the influence of the laser irradiation regimes applied to the alloy powder on the microstructure of the SLM-fabricated specimens. Alloy powders with the average diameter of 22.2  $\mu\text{m}$  were prepared by the water atomization process. The chemical composition of such powder is presented in the Table 3. It was used the following parameters of the SLM process: the laser power and scan spacing varied from 75 to 200 W and from 0.1 to 0.3 mm, respectively; the powder stacking thickness and the lasers can speed were fixed at 0.05 mm and 50  $\text{mm}\cdot\text{s}^{-1}$ , respectively. Figure 3 shows OM images of the SLM builds at various laser powers from 75 to 200 W and scan spacing from 0.1 to 0.3 mm. These images correspond to the transverse cross section normal to the building direction. As one can see in these images, the laser scan traces are clearly observed for all the laser parameters used. The higher the laser power and the larger the spacing, the wider traces were formed. The laser energy  $E$  was determined using the

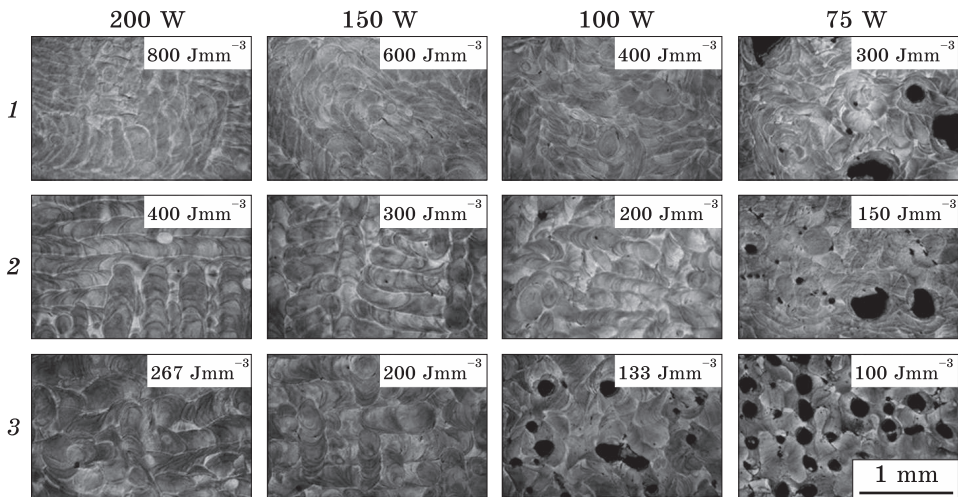


*Fig. 3.* OM images of the SLM fabricated samples for various laser powers (200 W, 150 W, 100 W, 75 W) and scan spacing (0.1 mm (1), 0.2 mm (2), 0.3 mm (3)) [46]

*Table 3.* Chemical composition of the water-atomized Co–29Cr–6Mo alloy powder (mas.%) [46]

Elements	Co	Cr	Mo	Si	Mn	Fe	Ni	C	O	N
Mas. %	Bal.	28.6	5.9	0.8	0.4	0.1	0.2	0.1	0.16	0.02

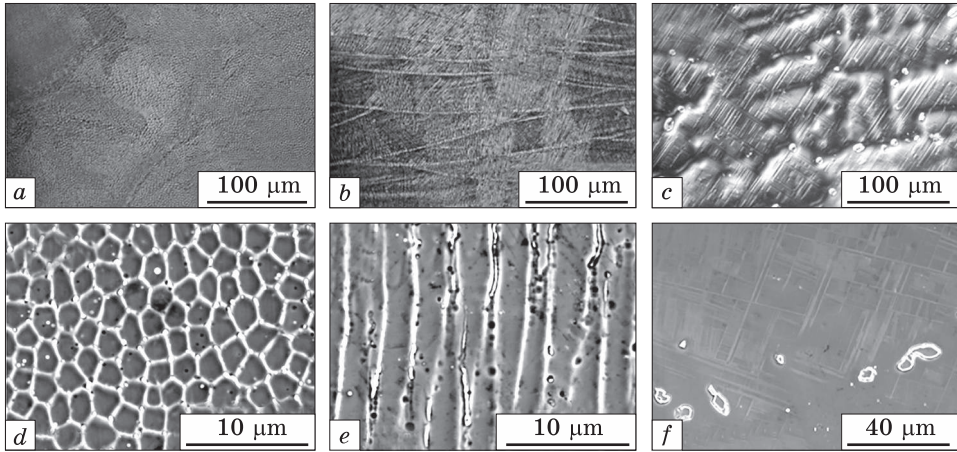


Fig. 4. Microstructures of the SLM and as-cast alloy samples: (a) OM image of 200 W to 0.1 mm taken from the transverse cross section normal to the building direction; (b) OM image of 200 W to 0.1 mm taken from the vertical cross section parallel to the building direction; (c) OM image of the as-cast alloy. SEM images of (d), (e), and (f) are magnified views of (a), (b), and (c), respectively [46]

following equation [47]:

$$E = \frac{P}{h\nu n},$$

where  $P$ ,  $h$ ,  $\nu$ , and  $n$  indicates the laser power (in W), the scan spacing (in mm), the scan rate (in  $\text{mm} \cdot \text{s}^{-1}$ ), and the layer thickness (mm), respectively. It can be noted that the dense samples were obtained when the laser energy was more than  $400 \text{ J} \cdot \text{mm}^{-3}$ . The porous samples were formed when the laser energy was less than  $150 \text{ J} \cdot \text{mm}^{-3}$  (Fig. 3). However, the influence of the laser power, overlapping ration, and scan spacing on the porosity should be noted. In particular, the samples produced at the laser energy range from 200 to  $300 \text{ J} \cdot \text{mm}^{-3}$  were not subject to the above tendency. The results indicate that the melted and densified zone for 200 W should be wider than 0.3 mm and that for 75 W was narrower than 0.1 mm. Accordingly, in addition to the input energy, the change of the energy distribution in the laser spot depending on the laser power should be taken into account. For comparison, Figure 4 demonstrates the microstructures of the SLM-produced and as-cast samples.

For the transverse cross-section normal to the SLM-building direction, OM image (Fig. 4, a) shows the circular arch-shaped boundaries and numerous fine particles. The SEM image shows that the latter includes cellular dendrites with the diameter of about 2.7 μm (Fig. 4, d). For the transverse cross-section parallel to the building direction, the OM image (Fig. 4, b) reveals the gradual arch-shaped boundaries almost normal to the building direction. It can be emphasized that the boun-

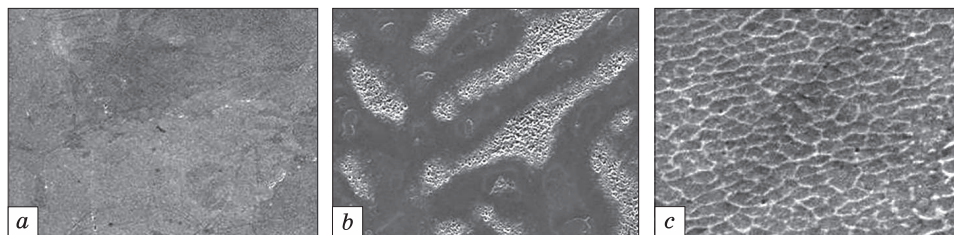


*Fig. 5.* SEM images fabricated by the (a) SLM ( $\times 1,000$ ) and (b) casting ( $\times 1,000$ ), where c — SLM sample ( $\times 10,000$ ) [49]

dary spacing almost corresponds to the stacking thickness of the powders (0.05mm). This observation indicates that the cellular dendrites were grown along the building direction. The microstructure of the as-cast alloy was different in comparison with those microscopic data related to the SLM processed sample. It consisted of the coarse dendrites with large particles (Fig. 4, c, f).

The phase compositions of the SLM-produced and cast samples were studied by x-ray diffraction. It was observed that for the cast samples fabricated with the pre-heated sand mould at 1073 K followed by cooling in air, both  $\gamma$ - and  $\varepsilon$ -phases coexisted in the alloy. Formation of the striations (Fig. 4, c) can be explained by the  $\gamma \rightarrow \varepsilon$  martensite transformation during cooling. The  $\gamma \rightarrow \varepsilon$  transformation in the Co–Cr–Mo alloy was reported to be susceptible to the grain size, and it was suppressed when the grain size was lower than 90  $\mu\text{m}$  [48]. Thus, at room temperature the SLM-built Co–29Cr–6Mo alloy sample predominantly contained the  $\gamma$  phase because the cross-sectional intercept length of the elongated grain size was about 33  $\mu\text{m}$ .

**2013.** The commercially available dental Co–Cr (Mo, W) alloy and its powder, containing (in wt.%) Co 61.5, Cr 26.0, W 5.0, and Mo 6.0 were studied in Ref. [46]. Several specimens were prepared from this alloy using a flame-cast method and oxygen–propane (50/50 v/v) gas mixture. The following parameters of laser were used for SLM: laser type — Nd:YAG; wavelength was 1.064  $\mu\text{m}$ ; pulse energy was 60 J; pulse length ranged 0.3–50 ms.

The features of the samples microstructure for two types are shown in Fig. 5, a, b, c. The cast sample ( $\times 1,000$ ) demonstrates one solid solution matrix and the crystalline phase in the typical dendritic formation. According to the local chemical analysis the ‘dark’ and ‘light’ areas of the microstructure showed the similar component. This indicates that these two areas belong to one solid solution matrix. It can be noted that ‘light in dark’ part showed the different component from ‘dark’ and ‘light’ parts which might indicate that this area belonged to the crystalline phase. Thereby, the microstructure of the casting samples is not

homogeneous (Fig. 5, *b*). On the other hand, the dendrite-like structural pattern, as well as the significant crystalline phase were not found in the SLM samples (Fig. 5, *a*). In fact, at magnification  $\times 10000$ , sample showed the cellular structure, which was homogeneous and regular, and the size of the cell is of about  $1\ \mu\text{m}$  (Fig. 5, *c*), and the grain size is much smaller than that of the cast samples.

The corrosion tests were performed using the electrochemical potentiostat *via* the test cell with the embedded specimen as the working electrode; the high-purity Pt wire was the counter electrode, and the Ag/AgCl reference electrode. To corrosion tests, the artificial saliva solution was used with next composition: NaCl — 0.1 g/L; KCl — 1.3 g/L; CaCl $_2$ ·2H $_2$ O — 0.1 g/L; MgCl $_2$ , 6H $_2$ O — 0.05 g/L; NaF — 0.000025 g/L; 0.5 g/L polypeptone; KH $_2$ PO $_4$  — 0.027 g/L; K $_2$ HPO $_4$  — 0.035 g/L (pH = 7.0), at  $37 \pm 0.5\ ^\circ\text{C}$ ). Table 4 shows the main parameters of the corrosion test: the corrosion current ( $I_{\text{corr}}$ ) and the polarization resistance ( $R_p$ ) of the SLM-built and cast specimens. The given data testify to the best anti-corrosion properties of the SLM-built specimens in comparison with those of the cast one. This confirms the good prospects for the use of SLM technique in dental clinics.

**2016.** The purpose of the study [50] was the comparative analysis of the microstructural characteristics of Co–Cr–W alloys fabricated using the commercial casting (CS) and SLM. The manufacturing process types, brand names and elemental compositions of the studied alloys are presented in Table 5.

Figure 6 shows the X-ray diffraction (XRD) patterns two Co–Cr–W alloy samples fabricated by casting and SLM. From these data it was identified the presence in the microstructure of the CS and SLM samples the Co-based f.c.c. ( $\gamma$ ) matrix structure with the nominal crystal lattice parameter  $a = 0.35447\ \text{nm}$ . However, there is the difference between the two groups of the samples. In particular, in the casting group, there are

Table 4. Corrosion parameters of SLM and cast specimens [49]

Specimens	$I_{\text{corr}},\ \mu\text{A}\cdot\text{cm}^2$	$R_p,\ \text{k}\Omega\cdot\text{cm}^2$
SLM	0.02	977.383
Cast	0.07	1129.9

Table 5. Manufacturing process, brand names and elemental compositions of the studied Co–Cr system alloys [50]

Process/Brand name	Co	Cr	W	Nb	V	Mo	Si	Fe
Casting/StarLoy C	59.4	24.5	10	2	2	1	1	0.1
SLM/Remanium® star CL	60.5	28	9	<1			1.5	<1

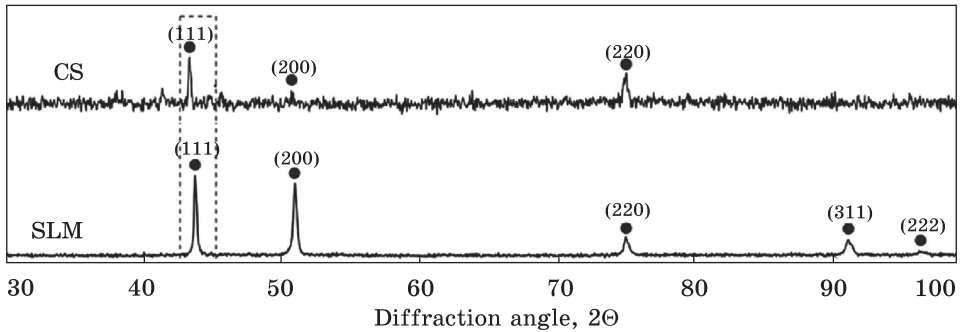


Fig. 6. XRD patterns of the Co–Cr–W samples fabricated by casting (CS) and 3D printing (SLM) [50]

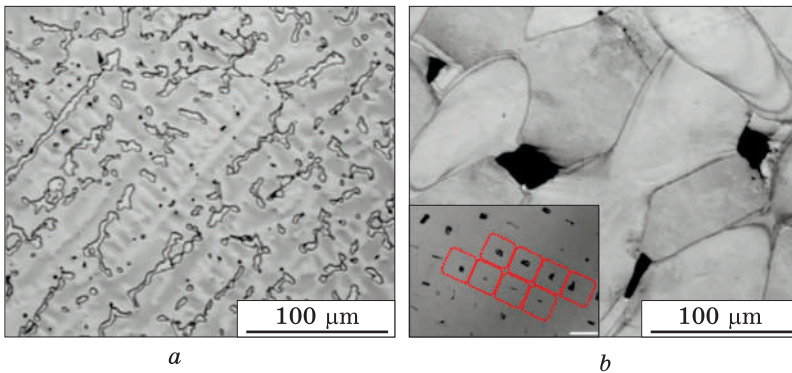


Fig. 7. OM images: *a* — casting sample; *b* — SLM sample [50]

two intermetallide phases assumed to be W-rich  $\varepsilon$  (h.c.p.) and Nb-rich  $\gamma$  (f.c.c.) phases together with the matrix phase. However, for the SLM group samples reflexes can be seen only for the Co-based  $\gamma$  f.c.c. phase.

The OM observations of microstructure of the samples fabricated by CS and SLM are presented in Fig. 7. It can be observed for the CS samples group that the typical dendritic grains are dominated as well as the precipitating intermetallic phases. It can also be noted that for the SLM samples the laser scan traces were clearly exhibited (see the small box in Fig. 7, *c*). Additionally, it can be noted that the energy dispersive x-ray spectrometry (EDS) clearly revealed the presence of the matrix, intermetallic, metal carbide phases and the silicon (Si-rich) inclusions for CS and SLM samples. However, the elemental distribution of the carbon was not detected.

**2017.** The surface morphology of the Co–Cr–(Mo, W) alloy specimens processed by slip-cast technique (CS) and SLM technique were investigated in Ref. [51]. Surface texture has important role in the manufacturing process. These data can be used as the way of gaining

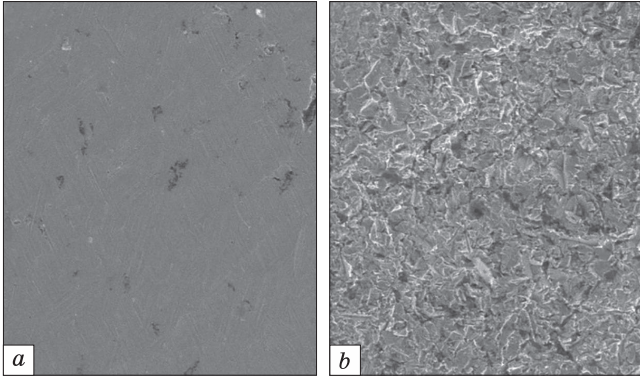


Fig. 8. EM images of the CS (a) and SLM samples (b) [51]

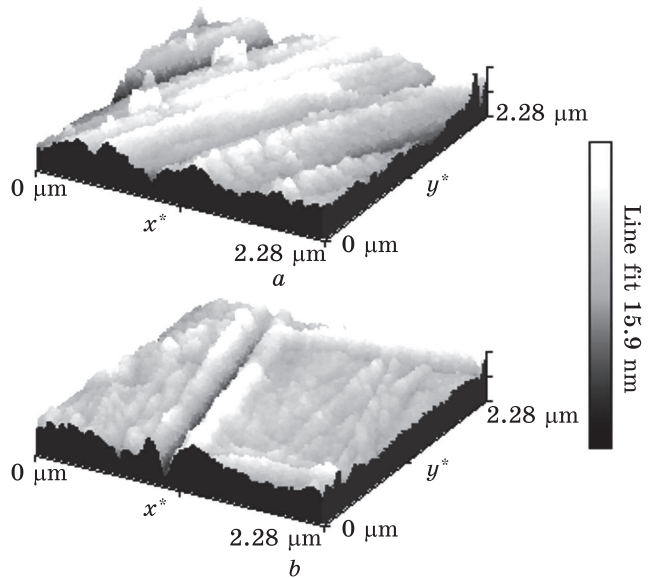


Fig. 9. AFM images of the surface CS (a) and SLM (b) samples [51]

insight into the physical phenomena taking place during the manufacturing process, through examination of the surface features generated by the process and the relation between the involved physical phenomena and the technique variables. CS specimens were manufactured in vacuum from wax discs sprue according to manufacturer indications. Composition of the CS specimens (wt.%): Co 62.07; Cr 28.64; Mo 3.82; W 2.02; Fe 3.45. After casting, the specimens sandblasted with 100  $\mu\text{m}$  glass pearls. The SLM specimens were obtained using the next Co–Cr atomized metal powder composition (wt.%): Co 59.0; Cr 25.0; W 9.5; Mo 3.5; Si < 1; others < 1.5. The SLM used the high-power laser (50 W,  $\lambda = 1070$  nm), with high-speed (80 units per 4 hours) capacity.

It was found that the surface morphology depends on the technology of the sample preparation. The CS-made samples have the similar

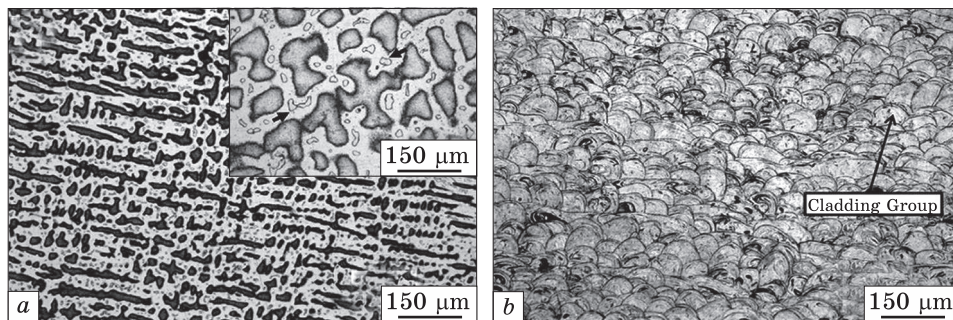


Fig. 10. OM images of polished sections: cast (a) and SLM (b) samples [36]

roughness as that of the SLM-built samples. However, the SLM sample has more irregular surface (Fig. 8). SEM shows the characteristic image of welding-lines (traces from melting of granules occurred during the sintering process). These granules suffer the rapid melting because of melt-pool that cools down and solidifies with the waved and rough texture [51]. The microstructures observed for the as-cast and SLM-built samples were found to be free of cracks or defects.

Figure 9 presents the AFM images of the surfaces of the CS-made (a) and SLM-built (b) samples. SLM without thermal posts-treatment shows the bumpy surfaces with open pores and higher peaks. The calculated surface average roughness was 35 nm after SLM and 7.4 nm after CS.

**2018.** The purpose of the work [36] was to investigate the dental Co–Cr–(W, Mo) alloys fabricated by casting and SLM. The alloy powder has the following composition (in wt.%): Co 63.9; Cr 24.7; W 5.7; Mo 5.0. The powders were spherical with the smooth surface with the sizes ranged 20–50  $\mu\text{m}$ . Cast samples demonstrated the composition (wt.%): Co 60.2; Cr 25.0; W 6.2; Mo 4.8; Ga 2.9 and other < 1.0.

The OM observations of the microstructures of the alloy specimens prepared using casting and SLM manufacturing techniques are shown in Fig. 10, a, b. It can be seen that the cast specimens exhibit typical dendritic microstructures that consisted of light and dark regions (Fig. 10, a). This typical dendritic structure is formed due to the low cooling rate (approximately 102 K/s) and the negative temperature gradient. The higher magnification allows revealing the existence of the several island-shaped intermetallic compounds and second-phase particles (inset in Fig. 10, a).

In contrast to the cast samples, the SLM specimens displayed superior microstructure. The SLM-induced local melting and rapid solidification minimized flaws and porosities. As the result, SLM process results in the dense material with homogeneous fine-grain microstructure. Hence, the average grain size of the SLM-built specimens was

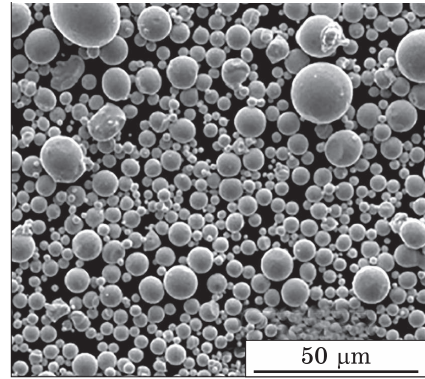
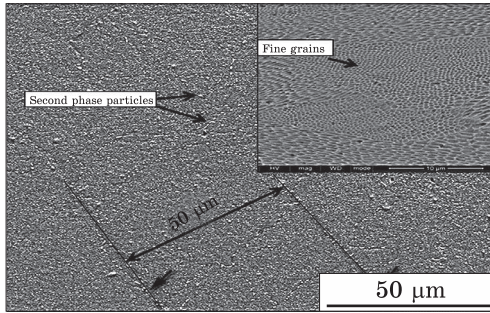


Fig. 11. SEM image of the SLM sample (original magnification  $\times 2000$  and magnification of insets  $\times 10000$ ) [36]

Fig. 12. SEM image of the Co-Cr-Mo-W alloy powder particles [52]

smaller than that of the cast specimens because the degree of the supercooling rate of the SLM-built samples significantly exceeded that of the cast specimens. The SLM specimens contained the large number of the homogeneously dispersed second-phase particles (Fig. 11) and had no dendritic segregations, but their microstructure was fine-grained and homogenous (Fig. 10). In order to observe the grains, the SLM specimens were also analysed by SEM. The SEM observations show that the second phase particles are distributed in the interior and at the boundary of the grains. The size of grains/sub-grains in the SLM specimens is within 1–5  $\mu\text{m}$  (Fig. 3). The cladding layer spacing is approximately 50  $\mu\text{m}$  (Fig. 3).

X-ray diffraction analysis was used to study the phase analysis of the fabricated samples. According to the x-ray spectra, the main phases in the cast specimens were  $\gamma$ -Co phase (f.c.c.) and  $\varepsilon$ -Co phase (h.c.p.). It was also shown that the weak reflex from the  $\sigma$  phase (an intermetallic compound) with the closely packed lattice was detected in the cast specimens. In the same time, the x-ray reflexes indicate the predominance of the  $\gamma$ -Co phase and much lower content of the  $\varepsilon$ -Co phase in the SLM-built samples. The XRD-based estimations have shown for both groups of the samples the following percentages of the f.c.c.  $\gamma$ -Co phase: 44% and 97% after casting and SLM, respectively.

**2020.** The comparative study of more complex Co-Cr alloy containing both Mo and W as the alloying elements was performed in the work

Table 6. Chemical content of the Co-Cr-Mo-W alloy (wt.%) [52]

Element	Co	Cr	Mo	W	Si	Nb
Content	Bal.	25.15	3.99	6.36	1.03	1.04

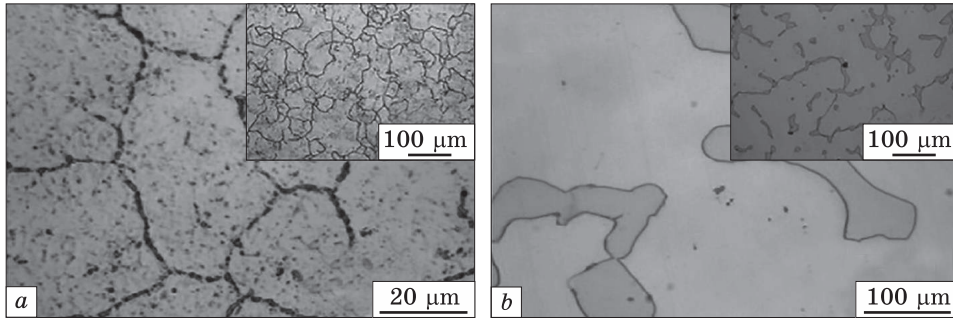


*Fig. 13.* OM images of samples fabricated by SLM (a) and casting (b) [52]

[52]. The alloy powders were produced by gas atomization in nitrogen atmosphere (Table 6). As the precursor materials, the cast Co–Cr–Mo–W alloy ingots were used. The SLM-built and cast Co–Cr–Mo–W alloy samples have almost the same chemical compositions. According to SEM image, the powder particles had spherical shape with size ranges from 12 to 45  $\mu\text{m}$  (Fig. 12). The following optimized processing parameters used to prepare the SLM samples: laser power was 180 W; scanning speed was 1400 mm/s; layer thickness was 35  $\mu\text{m}$ ; scan interval was 70  $\mu\text{m}$  and the hatch spacing was 150  $\mu\text{m}$  (30% overlap). For comparison of the microstructures, another group of samples was prepared by the sand mould casting.

According to x-ray analysis, the samples fabricated by SLM and casting were composed of the  $\epsilon$ -Co phase (h.c.p.),  $\gamma$ -Co phase (f.c.c.), and Laves phase (intermetallic compound). However, the SLM-built samples contained more  $\gamma$ -Co phase and relatively smaller contents of  $\epsilon$ -Co and Laves phase. The OM phase morphology of the microstructure of the SLM-built and cast samples revealed after electrochemical etching is presented in the Fig. 13, a, b. As can be seen, the SLM sample contains equiaxed grains with the sizes range from 20 to 50  $\mu\text{m}$  (Fig. 13, a). It is also seen that the striations of the HCP  $\epsilon$ -Co phase is not observed inside the SLM-built sample. The cast sample shows the large grain size (up to 300  $\mu\text{m}$ ) and island-like Laves phase precipitates (Fig. 13, b). More detailed SEM analysis showed the nanosize second Laves phase spread uniformly over the grain interior for the SLM-built samples. At the same time, the submicronic second phase precipitates (Laves phase) were distributed in the grain boundary and island-like Laves phase with the size larger than 10  $\mu\text{m}$  located at the gain boundary and the grain interior. For the cast samples, the island-like precipitates exhibited the dendritic shape.

**2020.** The purpose of the study [8] was to evaluate the microstructure of the SLM-fabricated Co–Cr alloys subjected to the subsequent post-process heat treatment. The experimental specimens were fabrica-

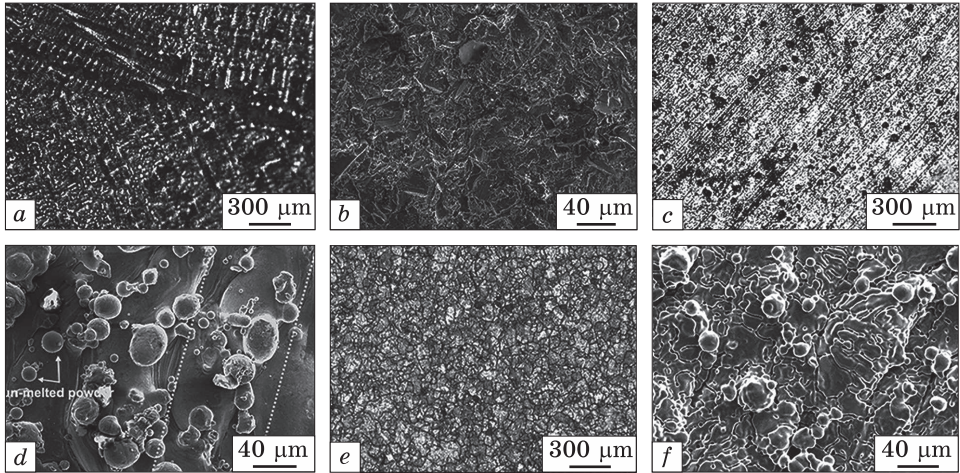


Fig. 14. OM images and SEM observations of the samples: *a* and *b* — cast; *c* and *d* — SLM; and *e* and *f* — heat treatment [8]

ted by means of the following manufacturing processes: lost-wax casting (CS group), SLM, and SLM followed by heat treatment (SLM-H group). The chemical compositions of the samples are listed in Table 7 according to the descriptions provided by the manufacturers. The following recommended SLM parameters were used: the laser power was 160 W; the laser scan speed was 1200 mm/s; the hatch distance was 0.03 mm; and the layer thickness was 70  $\mu\text{m}$ . For each condition, the longitudinal direction of the specimens was parallel to the building direction. After the SLM processes, a part of the specimens (the SLM-H group) were subjected to heat treatment in the furnace filled by high-purity Ar gas. The regime of the heat treatment was the following: specimens were heated from room temperature up to 1150  $^{\circ}\text{C}$  at the rate of 10  $^{\circ}\text{C}/\text{min}$  and held for 6 hours in the furnace. Thereafter, the specimens were slowly furnace cooled to room temperature.

Table 7. Nominal composition (wt.%) of Co–Cr samples [8]

Processes	Co	Cr	Mo	Ni	Fe	Mn
Casting	61.5	29.2	5.8	1	<1	<1
SLM	62.5	28.0	6.0	<0.1	0.75	<1

Table 8. Elemental compositions of Co–Cr samples (wt.%) [53]

Methods	Co	Cr	W	Mn	Fe	Nb	Si	Mo
Lost-wax casting	661.0	224.0	88.0	11.0	11.0	11.0	11.0	22.5
SLM	60.5	28.0	9.0	1.0	1.0	1.0	1.5	

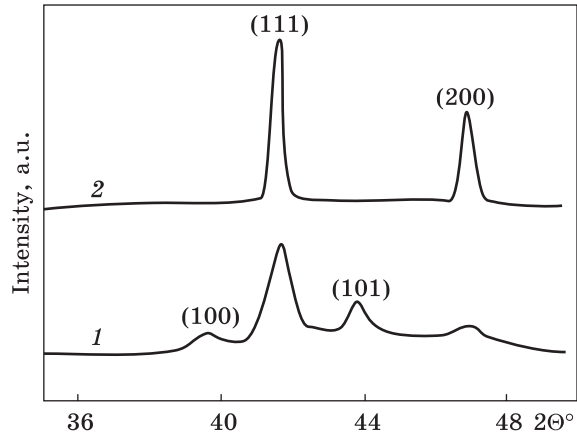


Fig. 15. X-ray patterns for casting (1) and SLM (2) [8]

Figure 14 shows the OM observations of microstructures that vary for different sample production methods (CS and SLM). For the cast samples, the coarse dendrite grains and ramifications with different orientations during solidification is typical (Fig. 14, *a*). Moreover, the CS sample contains casting porosity and the coarse microstructure with the grain sizes between approximately 818 and 1135  $\mu\text{m}$  (Fig. 14, *b*). The surface morphology of the SLM samples is different, it contains of the unclear grain boundaries and obvious melted tracks of approximately 70  $\mu\text{m}$  wide (Fig. 14, *c*). Additionally, the bright ripples were also seen. The large amount of nonmelted powder on the scale of tens of micrometres was randomly dispersed on the surfaces. There are several newly observed surface characteristics of the SLM specimens after heat treatment (Fig. 14, *e, f*). First, there are the well-defined grain boundaries with the grain sizes in the range 29–212  $\mu\text{m}$ . Additionally the unclear molten pool boundaries can also be observed. Figure 15 shows the XRD patterns of the CS-made and SLM-built samples. For CS samples, the mixture of the  $\gamma$  (f.c.c.) and  $\varepsilon$  (h.c.p.) phases is typical. Moreover, the weak diffraction reflex that belongs to the  $\sigma$  phase was also observed. In the same time, the  $\varepsilon$  phase had disappeared in both SLM and SLM-H specimens. Conversely, the  $\gamma$  phase was strong and clear. In the SLM-H specimens, the low-intensity reflexes of the  $\sigma$  phase were observed to be accompanied by remarkable peaks of the  $\gamma$  phase.

**2022.** The recent work [53] was aimed to study the surface microstructures and corrosion resistance of the dental Co–Cr–(Mo, W) alloys samples fabricated by the casting and SLM. The composition of the alloys presented in the Table 8. The casting samples were manufactured by the conventional lost wax technique. The following SLM regime was used: power of Yb-fibre laser was 100 W; the size of the Co–Cr powder was 10–40  $\mu\text{m}$ ; the building layer thickness was 25  $\mu\text{m}$ ; scan speed was 7 m/s, manufacturing speed was 5  $\text{cm}^3/\text{h}$  and the longitudinal axes of

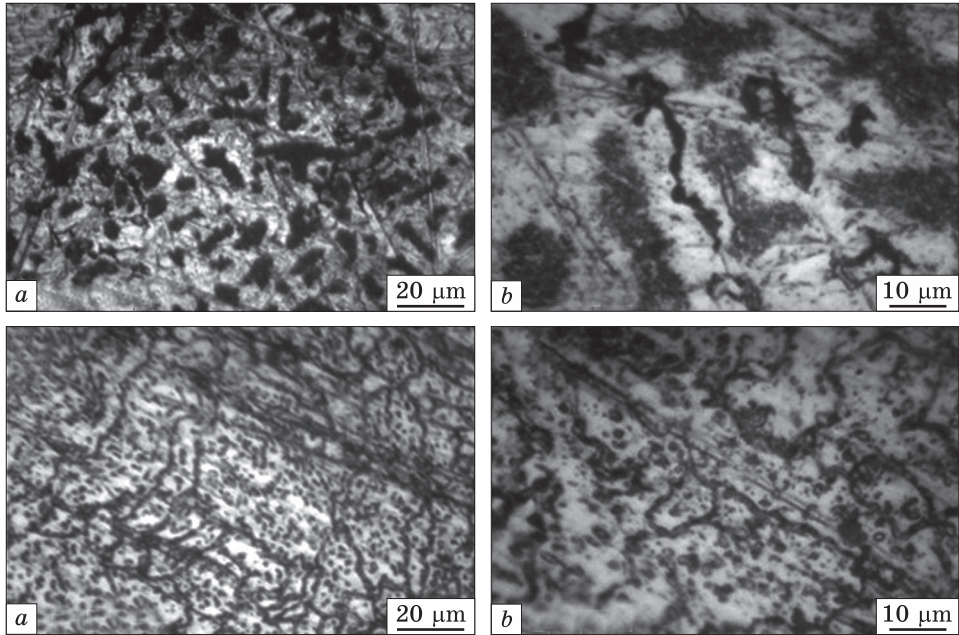


Fig. 16. SEM micrographs of the Co–Cr alloys samples fabricated by cast (a, b) and SLM (c, d) [53]

the specimens was parallel to the building platform. After fabricating, the SLM-built samples were subjected to the post-build heat treatment in a furnace to remove the residual stress arising from the local laser melting and to tailor the microstructure. The heat treatment was performed in the argon gas atmosphere at 1150 °C for 1 h with subsequent cooling down to the furnace temperature (200 °C).

The SEM observations of the microstructures of the Co–Cr alloys samples fabricated by two processes are shown in Fig. 16. The casting specimen demonstrates the typical inhomogeneous dendritic solidification microstructure consisting of dendrites and interdendritic areas with the grain size of about 20–100 μm (see the light and dark regions in Fig. 16, a, b). For the SLM specimen, the much finer homogeneous structure (the grain size of 2–20 μm) was observed, the compact finger-like peculiarities were covered with many scattered second phase particles which was dispersed randomly at the grain boundaries (Fig. 16, c, d). Additionally, the XRD analysis shows that the  $\epsilon$ -Co phase (h.c.p.) was identified additionally to the  $\gamma$ -Co phase (f.c.c.) in all specimens.

As shown recently, the pre-heating process can be useful for the enhancement of the microstructure and mechanical characteristics of the SLM-built specimens of CoCrMo alloy [54]. This study revealed that the increase of the pre-heating temperature not only decreases residual

stress, but also improves the mechanical characteristics of the SLM-built CoCrMo alloy. Additionally, rising pre-heating temperature results in the decrease in the volume fraction of the martensitic  $\varepsilon$ -Co phase. As the cooling speed increased, precipitation of the micro scale  $\varepsilon$ -Co phase was inhibited, which allowed the growth of the  $\gamma$ -Co f.c.c.-phase grain boundary. However, the high strength properties were maintained due to the unique lamellar-structure precipitates of the nanoscale martensitic  $\varepsilon$ -Co phase.

### **3. Conclusions**

One of the most important areas of the dentistry is prosthodontics, which is associated with replacing of the missing tooth/teeth. In connection with this, there are many different types of the metal alloys to be used in the dentistry. For the production of the metallic dental prostheses in the recent years, Co–Cr-based alloys are most on-demand alloys for various and successful clinical applications. Mo and W used as the powerful strengthening agents for these alloys with the high strength and stainless nature. The literature describes the properties of such alloys having of the main elements contents in the following ranges (in wt.%): Co 31–67; Cr 24–32; Mo 3–6; W 8–9. Addition of carbon makes the alloy highly wear resistant mainly due to precipitation of the  $M_{23}C_6$ ,  $M_7C_3$ , and  $M_6C$  carbides (where M represents Co, Cr, Mo or W). It is well known that the properties of the Co–Cr dental alloys depend on the ratio between  $\gamma$ (f.c.c.)/ $\varepsilon$ (h.c.p.) phases and the type, quantity and distribution of the carbide phase in the microstructure. To produce dental prostheses made of the Co–Cr-based alloys the lost-wax casting and hot forging processes are traditionally used. However, fabrication of the Co–Cr-based dental parts possessing simultaneously high strength and complex shape by conventional casting process is difficult task. Complexly shaped components can be produced by casting at the expense of their lowered strength, which retains not high enough.

Therefore, in order to solve these problems, the nowadays additive manufacturing (AM or 3D printing) is being developed as the effective way for fabrication of the customized dental prostheses. Such AM technology is receiving increasing attention around the world. Usually, AM technology creates 3D products layer by layer in a single stage directly from their 3D computer-aided design (CAD) by successively adding materials in a layer-by-layer fashion. Nowadays, the 3D printing of metals is popular in many industries since it allows printing the complex metal parts with the relatively low price as compared to the traditional manufacturing processes, in particular in the aerospace, automotive, marine, and military. Metal 3D printing also has uses in the medical sector such as in production of the implants and dental prosthetics.

Recent publications have shown that 3D printing provides the efficient and fast technique for digital design and manufacture biocompatible metal frameworks for complex dental prostheses with improved physical and chemical properties, such as strength, durability and corrosion resistance. Nowadays, such AM as the SLM process is the most frequently used to develop frameworks in dentistry to fabricate directly metallic dental medical parts from the alloys of the Co–Cr system. Studies have also shown that prostheses fabricated of Co–Cr alloys by the SLM process have better corrosion resistance and higher strength compared with those produced by using conventional casting methods. This is because, in contrast to the casting, the SLM process leads to the formation of the improved microstructure that further provides superior properties of the SLM-built products. Complete local melting and rapid solidification occurred during SLM have minimized the residual flaws and porosity. As a result, the SLM process results in the dense material with homogeneous fine-grained microstructure.

**Acknowledgement.** This work contains results carried out within the framework of the project of Ministry of Education and Science of Ukraine ‘Structural-phase control mechanisms of the complex of surface properties of structural and functional alloys by combined thermal, ionic and deformation influences’ (State Reg. No. 0121U109752).

## REFERENCES

1. W. Riaz, A. Ayesha, and S. Aziz, *Professional Med. J.*, **25**: 1261 (2018); <https://doi.org/10.29309/TPMJ/18.4488>
2. M.O. Vasylyev, I.M. Makeeva, and P.O. Gurin, *Prog. Phys. Met.*, **20**, No. 2: 310 (2019); <https://doi.org/10.15407/ufm.20.02.310>
3. M.O. Vasylyev, V.S. Filatova, I.M. Makeeva, and P.O. Gurin, *Metallofiz. Noveishie Tekhnol.*, **43**, No. 9: 1139 (2021); <https://doi.org/10.15407/mfint.43.09.1139>
4. E. Haynes, *Metal Alloy*, U.S.P. Office, Washington, DC, USA, 1907.
5. A.K. Mishra, M.A. Hamby, and W.B. Kaiser, *Metallurgy, Microstructure, Chemistry and Mechanical Properties of a New Grade of Cobalt–Chromium Alloy before and after Porous-Coating* (West Conshohocken, PA, USA: ASTM: 1999).
6. A. Marti, *Injury*, **31**, Suppl. 4: D18 (2000); [https://doi.org/10.1016/S0020-1383\(00\)80018-2](https://doi.org/10.1016/S0020-1383(00)80018-2)
7. Youssef S. Al Jabbari, *J. Adv. Prosthodont.*, **6**, No. 2: 138 (2014); <https://doi.org/10.4047/jap.2014.6.2.138>
8. A. Vaicelyte, C. Janssen, M. Le Borgne, and B. Grosogoeat, *Crystals*, **10**, No. 12: 1151 (2020); <https://doi.org/10.3390/cryst10121151>
9. M. Podrrez-Radziszewska, K. Haimann, W. Dudzinski, and M. Morawska-Soltysik, *Arch. Foundry Eng.*, **10**: 59 (2010).
10. P. Gupta, *J. Phase Equilibria and Diffusion*, **26**: 87 (2005); <https://doi.org/10.1361/15477030522608>

11. Yu.N. Petrov, G.I. Prokopenko, B.N. Mordyuk, M.A. Vasylyev, S.M. Voloshko, V.S. Skorodzievski, and V.S. Filatova, *Mater. Sci. Eng. C*, **58**: 1024 (2016); <https://doi.org/10.1016/j.msec.2015.09.004>
12. R. Liu, X.Y. Li, X. Hu, and H.S. Dong, *Surf. Coat. Technol.*, **232**: 906 (2013); <https://doi.org/10.1016/j.surfcoat.2013.06.122>
13. H. Nesse, D.M.A. Ulstein, M.M. Vaage, and M. Filo, *J. Prosthet. Dent.*, **114**: 686 (2015); <https://doi.org/10.1016/j.prosdent.2015.05.007>
14. E.-H. Kim, D.-H. Lee, S.-M. Kwon, and T.-Y. Kwon, *J. Prosthet. Dent.*, **117**: 393 (2016); <https://doi.org/10.1016/j.prosdent.2016.08.002>
15. R. Van Noort and M. Barbour, *Introduction to Dental Materials* (Elsevier Health Sciences: 2014).
16. B. Berman, *Business Horizons*, **55**: 155 (2012); <https://doi.org/10.1016/j.bushor.2011.11.003>
17. P. Wu, J. Wang, and X. Wang, *Automat. Constr.*, **68**: 21 (2016); <https://doi.org/10.1016/j.autcon.2016.04.005>
18. B. Bhushan and M. Caspers, *Microsyst. Technol.*, **23**: 1117 (2017); <https://doi.org/10.1007/s00542-017-3342-8>
19. D. Ngo Tuan, A. Kashani, G. Imbalzano, T.Q. Nguyen Kate, and D. Hui, *Composites, Part B*, **143**: 172 (2018); <https://doi.org/10.1016/j.compositesb.2018.02.012>
20. D.L. Rakov and R.Y. Sukhorukov, *J. Mach. Manuf. Reliab.*, **50**: 616 (2021); <https://doi.org/10.3103/S1052618821070116>
21. M. Srivastava, S. Rathee, S. Maheshwari, and T. K. Kundra, *Additive Manufacturing: Fundamentals and Advancements* (Taylor & Francis Group: 2019).
22. B. Dylan, F. Jeffrey, S. Gregory, and A. Ehssan, *The Future of Additive Manufacturing in the U.S. Military* (A Research Report Submitted to the Faculty in Partial Fulfillment of the Graduation Requirements Advisor: Dr. Paul J. Springer 17 Mar 2017).
23. H. Kodama, *Rev. Sci. Instrum.*, **52**: 1770 (1981); <https://doi.org/10.1063/1.1136492>
24. P. Ciraud, *Verfahren und Vorrichtung zur Herstellung Beliebiger Gegenstände aus Beliebigen Schmelzbarem Material* [Process and Device for the Manufacture of Any Object from Any Fusible Material]: German Patent DE 2263777, priority filed December 28, 1971, published July 5, 1973.
25. R. Housholder, *Molding Process*, US Patent 4247508, filed December 3, 1979, published January 27, 1981.
26. P.M. Pragana, R.F.V. Sampaio, I.M.F. Braganza, C.M.A. Silva, and P.A.F. Martins, *Adv. Industrial Manuf. Eng.*, **2**: 100032 (2021); <https://doi.org/10.1016/j.aime.2021.100032>
27. J.D. Buchbinder, H. Schleifenbaum, S. Heidrich, W. Meiners, and J. Bultmann, *Phys. Procedia*, **12**: 271 (2011); <https://doi.org/10.1016/j.phpro.2011.03.035>
28. E. Costa Santos, M. Shiomi, K. Osakada, and T. Laoui, *Int. J. Machine Tools & Manufacture*, **46**: 1459 (2006); <https://doi.org/10.1016/j.ijmachtools.2005.09.005>
29. M. Gupta, *Metals*, **7**: 403 (2017); <https://doi.org/10.3390/met7100403>
30. C. Buchanan, V.-P. Matilainen, A. Salminen, and L. Gardner, *J. Construct. Steel Res.*, **136**: 35 (2017);

- <http://dx.doi.org/10.1016/j.jcsr.2017.05.002>
31. B. Vandenbroucke and J. P. Kruth, *Rapid Prototyping J.*, **13**: 196 (2007);  
<https://doi.org/10.1108/13552540710776142>
  32. L. Ardelean, L. Reclaru, C. Bortun, B. Ghiban, and L.C. Rusu, *Metalurgia Int.*, **15**: 31 (2010).
  33. W.-F. Lee, J.-C. Wang, C.-Y. Hsu, and P.-W. Peng, *J. Prosthetic Dentistry*, **127**: 115 (2022);  
<https://doi.org/10.1016/j.prosdent.2020.06.038>
  34. R. Van Noort, *Dent. Mater.*, **28**: 3 (2012);  
<https://doi.org/10.1016/j.dental.2011.10.014>
  35. W. Wei, Y. Zhou, W. Liu, N. Li, I. Yan, and H. Li, *J. Mater. Eng. Perform.*, **27**: 5312 (2018);  
<https://doi.org/10.1007/s11665-018-3520-6>
  36. Y. Zhou, N. Li, J. Yan, and Q. Zeng, *J. Prosthetic Dentistry*, **120**: 617 (2018);  
<https://doi.org/10.1016/j.prosdent.2017.11.015>
  37. M. Kassapidou, L. Hjalmarsson, C.B. Johansson, P.H. Johansson, E. Morisbak, A. Wennerberg, and V.F. Stenport, *Dental Mater.*, **36**, No. 11: e35236 (2020).  
<https://doi.org/10.1016/j.dental.2020.08.012>
  38. H.T. Im, D.H. Kim, Y.D. Kim, J.O. Fadonougbo, C. Bin, J.-Y. Park, K.B. Park, J.-W. Kang, H.-S. Kang, and H.-K. Park, *Mater. Characterization*, **186**: 111767 (2022);  
<https://doi.org/10.1016/j.matchar.2022.111767>
  39. T. Barbin, D.V. Veloso, L. Del Rio Silva, G.A. Borges, A.G.C. Presotto, V.A.R. Barão, and M.F. Mesquita, **108**: 103821 (2020);  
<https://doi.org/10.1016/j.jmbbm.2020.103821>
  40. E.D. Rekow, *Dental Mater.*, **36**: 9 (2020);  
<https://doi.org/10.1016/j.dental.2019.08.10>
  41. T. Koutsoukis, S. Zinelis, G. Eliades, K. Al-Wazzan, and M.A. Rifaiy, Y.S. Al Jabbari, *J. Prosthodont.*, **24**, No. 4: 303 (2015);  
<https://doi.org/10.1111/jopr.12268>
  42. K.P. Krug, A.W. Knauber, and F.P. Nothdurft, *Clin. Oral Investig.*, **19**: 401 (2015);  
<https://doi.org/10.1007/s00784-014-1233-2>
  43. M. Revilla-León and M. Özcan *Curr. Oral Health Rep.*, **4**: 201 (2017);  
<https://doi.org/10.1007/s40496-017-0152-0>
  44. F.Y. Liao, G. Chen, C.X. Gao, and P.Z. Zhu, *Adv. Eng. Mater.*, **4**: 1801013 (2019);  
<https://doi.org/10.1002/adem.201801013>
  45. <https://www.bego.com>
  46. A. Takaichi, Suyalatu, T. Nakamoto, N. Joko, N. Nomura, Y. Tsutsumi, S. Migita, H. Doi, S. Kurosu, A. Chiba, N. Wakabayashi, Y. Igarashi, and T. Hanawa, *J. Mech. Behavior Biomed. Mater.*, **21**: 67 (2013);  
<https://doi.org/10.1016/j.jmbbm.2013.01.021>
  47. A. Simchi, *Mater. Sci. Eng. A*, **428**: 148 (2006);  
<https://doi.org/10.1016/j.msea.2006.04.117>
  48. P. Huang and H. F. Lopez, *Mater. Lett.*, **39**: 249 (1999);  
[https://doi.org/10.1016/S0167-577X\(99\)00022-1](https://doi.org/10.1016/S0167-577X(99)00022-1)
  49. X.-Z. Xin, J. Chen, N. Xiang, and B. Wei, *Cell Biochem. Biophys.*, **67**: 983 (2013);  
<https://doi.org/10.1007/s12013-013-9593-9>
  50. H.R. Kim, S.-H. Jang, Y.K. Kim, J.S. Son, B.K. Min, K.-H. Kim, and T.-Y. Kwon, *Mater.*, **9**: 596 (2016);  
<https://doi.org/10.3390/ma9070596>

51. C.E. Savencu, L. Porojan, M. Bordeanu, A. Boloş, S. Porojan, A. Antoniac, and S. Gradinaru, *Defect Diffus. Forum*, **376**: 1 (2017);  
<https://doi.org/10.4028/www.scientific.net/DDF.376.1>
52. X. Dong, Y. Zhou, Q. Sun, Y.T. Qu, H.J. Shi, W.B. Liu, H.B. Peng, B. Zhang, S. Xu, J. Yan, and N. Li, *Mater. Sci. Eng. A*, **795**: 140 000 (2020);  
<https://doi.org/10.1016/j.msea.2020.140000>
53. X. Xing, Q. Hu, Y. Liu, Y.H. Wang, and H. Cheng, *J. Prosthetic Dentistry*, **127**: 497 (2022);  
<https://doi.org/10.1016/j.prosdent.2021.11.019>
54. G.B. Bang, J.H. Park, W.R. Kim, S.-K. Hyun, H.-K. Park, T. W. Lee, and H.G. Kim, *Mater. Sci. Eng. A*, **841**: 143020 (2022);  
<https://doi.org/10.1016/j.msea.2022.143020>

Received 25.03.2022;  
in final version, 15.04.2022

*М.О. Васильєв*<sup>1</sup>, *Б.М. Мордюк*<sup>1,2</sup>, *С.М. Волошко*<sup>2</sup>, *П.О. Гурин*<sup>3</sup>

<sup>1</sup> Інститут металофізики ім. Г.В. Курдюмова НАН України,  
бульв. Акад. Вернадського, 36, 03142 Київ, Україна

<sup>2</sup> Національний технічний університет України  
«Київський політехнічний інститут імені Ігоря Сікорського»,  
просп. Перемоги, 37, 03056 Київ, Україна

<sup>3</sup> Національний університет охорони здоров'я України імені П.Л. Шупика,  
вул. Дорогожицька, 9, 04112 Київ, Україна

#### МІКРОСТРУКТУРА СТОМАТОЛОГІЧНИХ СТОПІВ Co–Cr, ВИГОТОВЛЕНИХ МЕТОДОМ ЛИТТЯ ТА 3D-СЕЛЕКТИВНОГО ЛАЗЕРНОГО ТОПЛЕННЯ

В огляді аналізується мікроструктура зразків комерційних стоматологічних стопів Co–Cr–(Mo, W), виготовлених за допомогою технології 3D-цифрового селективного лазерного топлення (SLM), що є найперспективнішою серед новітніх технологій адитивного виробництва, яких використовують для виготовлення металевих виробів у стоматології. У зв'язку з цим головною метою є порівняння мікроструктур металевих зуботехнічних виробів, виготовлених за двома технологіями виробництва, а саме, звичайним литтям та SLM. Розглядаються останні дослідження, опубліковані впродовж періоду 2013–2022 рр. Мікроструктура оцінювалася за допомогою оптичної мікроскопії (ОМ), сканувальної електронної мікроскопії з енергодисперсійною Рентгеновою спектроскопією (SEM–EDS), Рентгенової дифрактометрії (XRD), аналізу дифракційної картини зворотнього розсіяння електронів (EBSD) та атомно-силової мікроскопії (АСМ). Аналіз мікроструктури уможливіє зробити висновки щодо придатності технології SLM для стоматологічних застосувань. Показано, що мікроструктура денгальних стопів Co–Cr залежить від хімічного складу зразків, а також від параметрів застосованої технології виготовлення. Експериментальні результати довели, що, на відміну від литих зразків, зразки SLM демонструють поліпшену мікроструктуру за рахунок повного локального топлення та швидкого твердіння. Крім того, технологія SLM зводить до мінімуму залишкові дефектність і поруватість. В результаті SLM уможливіє формування щільного матеріалу з однорідною дрібнозернистою мікроструктурою.

**Ключові слова:** технології адитивного виробництва, 3D-лазерне топлення, мікроструктура, стопи Co–Cr, стоматологія.